ELSEVIER

Polymer 42 (2001) 5013–5021

polymer

www.elsevier.nl/locate/polymer

Overlapping of different rearrangement mechanisms upon annealing for solution-crystallized polyethylene

H. Matsuda, T. Aoike, H. Uehara*, T. Yamanobe, T. Komoto

Department of Chemistry, Gunma University, Kiryu, Gunma 376-8515, Japan

Received 10 July 2000; received in revised form 23 October 2000; accepted 27 November 2000

Abstract

The lamellar rearrangement upon annealing has been studied by a combination of differential scanning calorimetry (DSC), small-angle X-ray scattering (SAXS) analysis, and transmission electron microscopy (TEM) observation for solution-crystallized samples of a linear polyethylene having a narrow molecular weight distribution. The initial unannealed sample showed the regular stacking of single crystal lamellae of ~12 nm thickness, but showed double melting peaks, independent of the measured heating rate (HR). Each of the endotherms corresponds to the melting of initial lamellae and that of the crystals reorganized during DSC heating, respectively. The annealing behavior of the sample was significantly affected by both the annealing temperature and the time. A low-temperature annealing at 115°C, which is below the peak temperature of the former endotherm, *slowly* thickened the whole lamellae without any melting including partial or local lamellae. Increasing the annealing temperature (T_a) induces the other type of lamellar rearrangement mechanism where the lamellae *rapidly* thicken with the cooperative partial melting upon annealing. This rearrangement causes lamellar doubling behavior, showing a thickening of about twice, which was confirmed on TEM observation of the annealed samples. Because these doubled lamellae increased at the higher T_a, the lateral continuity of the initial lamellar stacking was lost. The DSC results revealed that these two different rearrangement mechanisms competitively coexist upon annealing over 120°C. Their balance predominantly depends on T_a. Correspondingly, the SAXS results indicate that the initial periodicity of the crystal/amorphous arrangement within the lamellar stacking morphology is lost at the middle T_a range of 123°C, where these two types of lamellar reorganization overlap. At the higher T_a range of 126°C, only a doubly rearranged lamellar structure remains, which causes an increase in the SAXS peak intensity.

Keywords: Polyethylene; Rearrangement; Transmission electron microscopy

1. Introduction

The rearrangement system for the semi-crystalline polymers has been discussed for decades. Several models [1,2] were proposed for the interpretation of the morphological changes on annealing. The initial morphology of the sample significantly affects the annealing behavior. For the melt-crystallized spherulite morphology, the induced entanglement prevents the stems from sliding along the longitudinal chain direction within the crystalline lamellae [3], thus effective annealing simply causes melt-recrystallization at T_a or on cooling from T_a.

In contrast, for the less entangled solution-crystallized polyethylene (PE), the lamellar thickening primarily occurs. Even for a linear ultrahigh molecular weight PE, Rastogi et al. [4] have recently reported that the stacked lamellar morphology of the solution-crystallized material exhibited a significant lamellar doubling in the longitudinal (thickness) direction on annealing. They concluded that this process is not necessarily accompanied by the melting of the sample during annealing. Earlier, Spells and co-workers [5–7] have also shown that the lamellar thickening during the annealing of a solution-grown crystal mat could occur with no melting, depending on the conditions, e.g. annealing temperature and heating rate up to the given temperature.

Such lamellar thickening has sometimes been regarded as a melt-recrystallization system [8–11], which is usual for the annealing of a melt-crystallized morphology [12,13]. When the melted portion was limited, this type of melting during annealing is called “local” or “partial” melting [14–17]. Anyhow, the viewpoints of these annealing models are concentrated on the possible melting during annealing.

In most cases, these rearrangement mechanisms are based on the results obtained by small-angle X-ray [4,7,9,10,12,13] or neutron scattering [5,17,18] and Raman measurements [19,20]. For the scattering data analysis, the repeating periodicity of the two phases having

* Corresponding author. Tel.: +81-277-30-1332; fax: +81-277-30-1333.
E-mail address: uehara@chem.gunma-u.ac.jp (H. Uehara).

0032-3861/01/$ - see front matter
PII: S0032-3861(00)00893-4

different electron densities is a key. Thus, they always provide lamellar information including not only the crystalline region but also the amorphous layers. In other words, decreasing scattering intensity during annealing has two possibilities: partial melting or a lack of lamellar stacking periodicity [7].

A big advantage of the electron microscopic observation lies in its direct characterization of the lamellar arrangement within the sample. If different lamellar morphologies coexist, the scattering data provide an average of the mixed information of these several systems. However, the morphological analysis by electron microscopy can evaluate these different systems individually.

Differential scanning calorimetry (DSC) measurements may also provide quantitative information on the annealing behavior if their endothermic peaks are split into several portions corresponding to the melting of the crystalline lamellae created through different annealing mechanisms. This means that a very sharp endotherm, that is a high peak resolution, is necessarily required for the analysis of the annealing effect based on DSC data. For this purpose, a linear PE having a narrow molecular weight (MW) distribution was selected in this work to obtain the homogeneity of the initial lamellar morphology within the starting material. The accuracy of the temperature in the DSC measurements may be advantageous for clarifying what occurs on annealing at a critical annealing temperature of 120–126°C for the solution-crystallized PE, where several annealing systems have been independently proposed by the different investigators [4–12,16,17].

In this work, the lamellar rearrangement upon annealing has been studied by a combination of DSC, small-angle X-ray scattering (SAXS) measurements and transmission electron microscope (TEM) observations for the solution-crystallized samples of a linear PE having a narrow MW distribution. The results obtained under the given conditions, including the annealing temperature and the time, were compared.

2. Experimental section

2.1. Sample preparation

The material tested was a linear PE with a narrow MW distribution, supplied by the National Institute of Standards and Technology (Lot SRM1483). Its weight and number average molecular weight were 3.2 and 2.9×10^4, respectively.

A 0.01 wt% dilute *p*-xylene solution of the sample PE was prepared at the boiling point under a nitrogen gas flow. This polymer concentration is much lower than the chain overlapping one calculated for the MW range of $\sim 3 \times 10^4$. The hot solution was cooled to 80°C to precipitate crystals. The crystal suspension was again heated slowly to 120°C to obtain a homogeneous solution with stabilized nuclei, followed by isothermal crystallization at 82°C. A sedimented mat of polyethylene single crystals was obtained by slowly filtering the crystal suspension, followed by drying in vacuo at room temperature (RT).

2.2. Annealing procedure

A Perkin–Elmer Pyris 1 DSC was used to perform the isothermal annealing in a cell. A piece of the sample mats (ca. 0.5 mg) sealed in a pan was heated to the annealing temperature (T_a) at a high heating rate (HR) of 200°C/min, followed by holding isothermally for a given annealing time (t_a). After annealing, the sample pan was rapidly cooled to RT at the same high rate of 200°C/min.

2.3. Measurements

The melting behavior of the unannealed and annealed materials was analyzed by the same Perkin–Elmer Pyris 1 DSC. The DSC heating scan was recorded to 180°C at a HR of 5–40°C/min under a nitrogen gas flow. Calibration of the DSC characteristics, including the melting temperature and heat of fusion, was made using indium and tin standards at each HR. The baseline subtraction was always done to eliminate equipment noise.

For the TEM observations, the JEOL 1200EXS electron microscope used was operated at 80 kV. The samples were stained by RuO_4 vapor and embedded in epoxy resin. The assembly was cut into thin sections of 60 nm thickness, using a Reichert UltraCut S. microtome.

The SAXS patterns were recorded on Rigaku type small-angle vacuum camera and imaging plate system. CuK_α radiation was generated at 40 kV and 150 mA by a Rigaku Type RU-200 rotating anode X-ray generator, which was monochromatized with a graphite monochrometer. An imaging plate pattern was recorded with the incident beam parallel to the mat surface. The exposure time was always 6 h. The scattering diagrams were reduced from the imaging plate patterns, using a Rigaku type *R*-axis reading system. All of the SAXS measurements were made at RT after the desired annealing.

3. Results

3.1. Melting behavior of the initial morphology

The melting behavior of the semi-crystalline material is often affected by several factors, including initial morphology, heating rate, and so on. Fig. 1 shows the HR dependence of the DSC melting curves for an unannealed solution-crystallized mat. The double melting peaks were observed at any HR. With increasing HR, the melting curve gradually broadens but the balance between these peaks exhibits insignificant change; the relative areas of low- and high-temperature peaks maintained their constant values. Similar DSC results have been reported by Manley

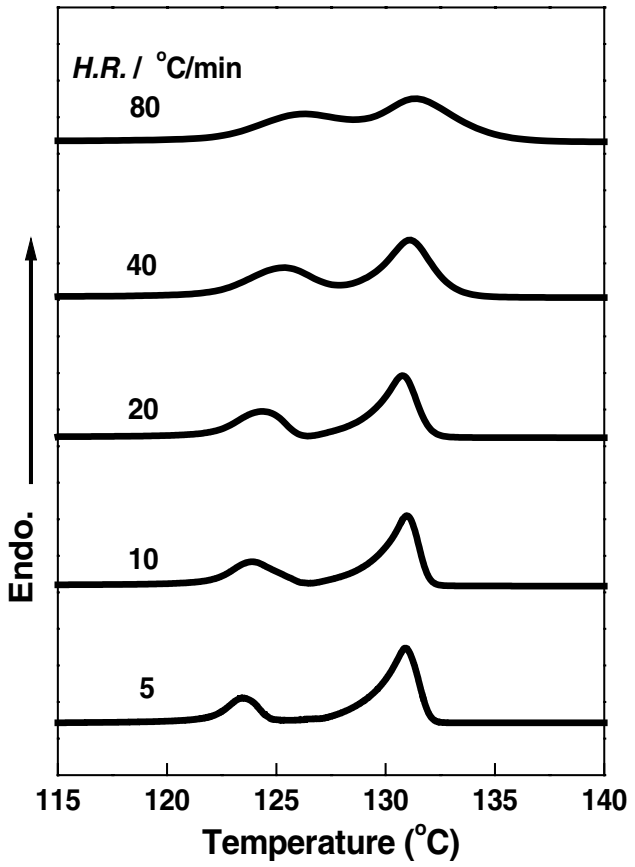

Fig. 1. DSC thermograms recorded at different HRs for initial solution-crystallized mat.

and co-workers [21] for the solution-crystallized low MW PE. These low- and high-temperature peaks are regarded as the melting of initially present lamellae and that of the crystals reorganized during the DSC heating scan, respectively. Otherwise, normal high density PE having a broad MW distribution shows a broadening of endotherms, which causes these two peaks to merge. A detailed discussion of the HR dependence of the melting behavior for the initial mats will be given in the next section.

The highest peak resolution could be obtained at the lowest HR of 5°C/min among those examined in this work. Thus, this HR was chosen for all other DSC experiments described below.

3.2. Annealing effects on the melting behavior

The melting behavior of the solution-crystallized mat was significantly affected by the given annealing conditions, i.e., annealing temperature and time. Fig. 2A exhibits DSC thermograms of the samples annealed for 1 min at different T_as. With increasing T_a, the initial double melting peaks gradually changed and merged into a single peak endotherm. Annealing at $T_a = 115$°C caused a low-temperature peak shift to the high-temperature side, but the high-temperature peak retained its position. The relative peak areas of these two peaks do not change. At $T_a = 120$°C, such a peak shift of the low-temperature peak is accelerated. Additionally, another difference lies in the slight appearance of a new peak located near 128°C between the low- and high-temperature peaks at $T_a = 120$°C. Clearer evidence of this new peak can be confirmed on the profile at $T_a = 120$°C in Fig. 2C showing the 30-min annealing results. In this paper, this peak between the initial double melting endotherm is called "middle-temperature peak". Here, the appearance of this middle-temperature peak could not be recognized at $T_a \leq 115$°C for any annealing time series examined in this work.

From $T_a = 120$ to 122°C, the area of this middle-temperature peak slightly increases at the higher T_a in Fig. 2A (the growth of this middle-temperature peak at this T_a range is more attractive for the 30-min annealing results in Fig. 2C). The slight shift into the low-temperature side for the high-temperature peak in this T_a range can be ascribed to the

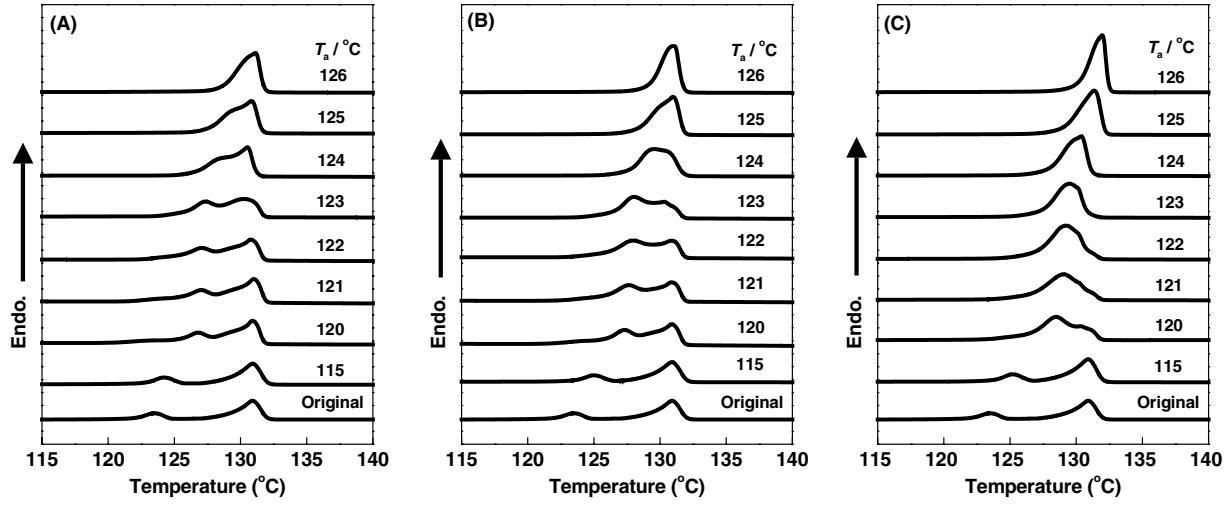

Fig. 2. Comparison of the DSC melting behavior for the solution-crystallized mat annealed at different T_a for: (A) 1 min; (B) 5 min; and (C) 30 min. The observed HR was 5°C/min. The thermograms of the unannealed samples are also included as a reference.

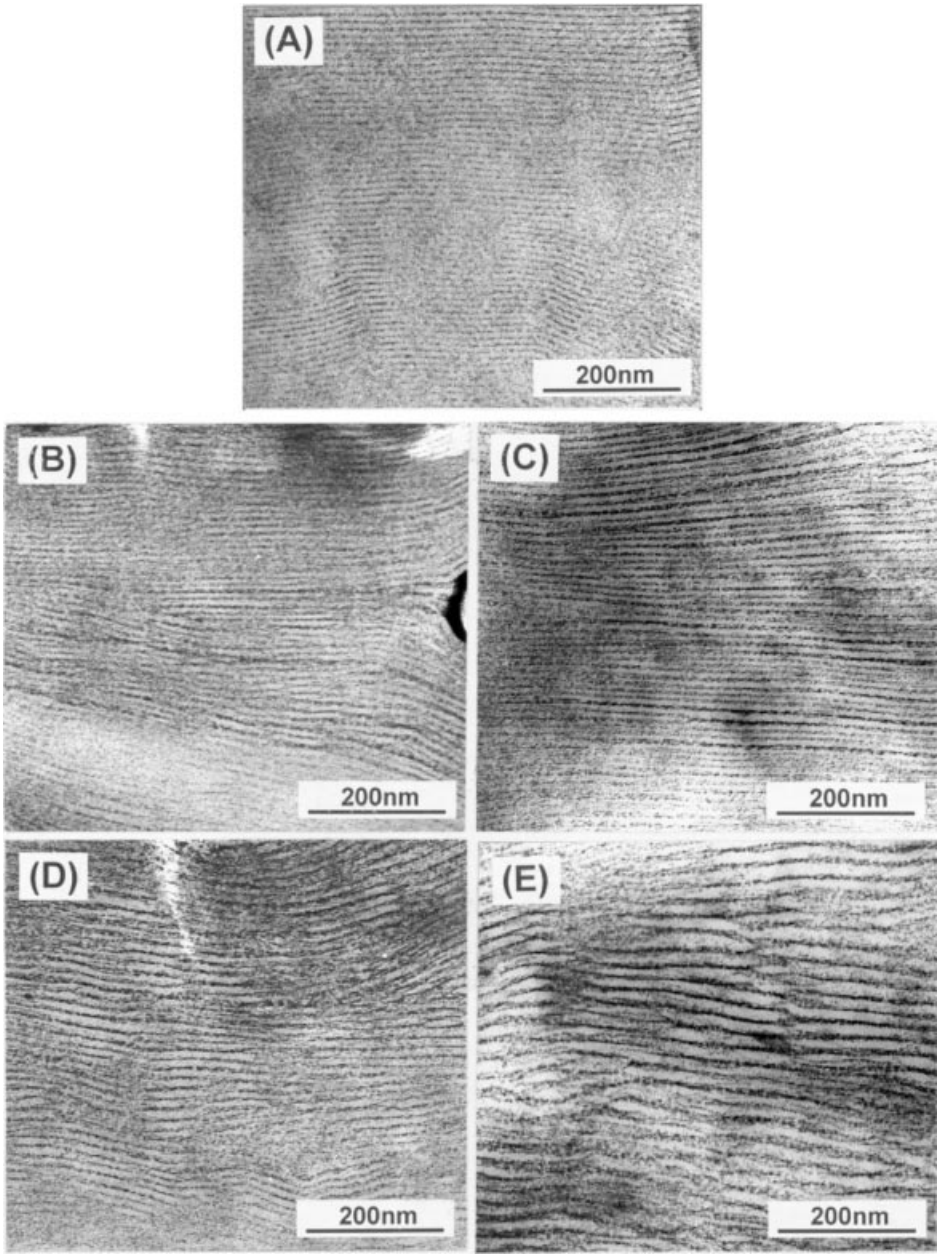

Fig. 3. TEM images of an initial unannealed mat and the sample annealed at different T_as for 1 min. These annealing conditions are comparable to those in Fig. 2. The result for an unannealed sample is also included as a reference: (A) Original; (B) $T_a = 115$°C; (C) 120°C; (D) 123°C; (E) 126°C.

nominal merging of such grown middle- and high-temperature peaks, due to the similar peak heights of both peaks as shown at $T_a = 123$°C in Fig. 2A. The low-temperature peak also exhibits a slight peak shift into the high-temperature side.

At $T_a = 124$°C in Fig. 2A, the drastic endotherm change is visible. The recorded endotherm has only double melting peaks which lie around 127 and 130°C. Taking into account the gradual endotherm change described above, the melting peak located around 130°C corresponds to the middle-temperature peaks observed at the lower T_as. In other words, there is no high-temperature peak at $T_a = 124$°C. The position of middle-temperature peak still shifts to the high-temperature side at further higher T_as of 125 and 126°C. The shift of the low-temperature peak is more rapid, thus, these two peaks appear merged. Even at $T_a = 126$°C, the predominant peak is the middle-temperature one which lies around 131°C.

The other series of the effect of T_a on the melting behavior of the annealed materials was compared for different t_as of 5 and 30 min. The obtained profiles are shown in Fig. 2B and C, respectively. The changes in the endotherm shape with T_a for 5-min annealing in Fig. 2B is similar to that of 1-min annealing in Fig. 2A. In contrast, the 30-min annealing

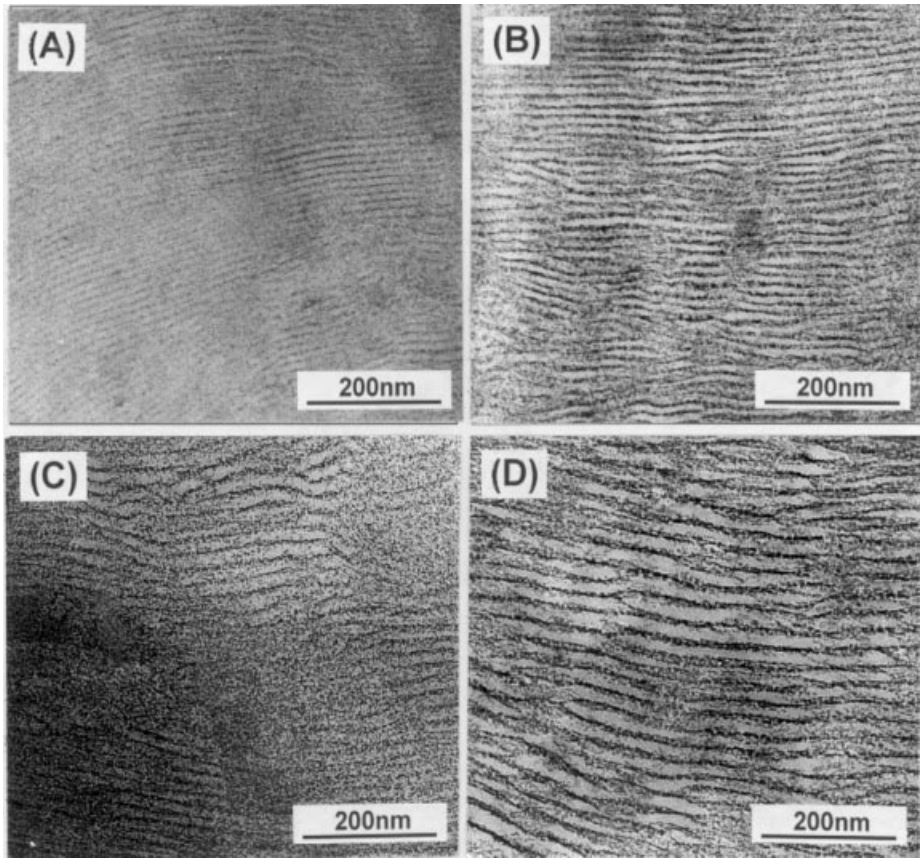

Fig. 4. TEM images of the sample annealed at different T_as for 5 min. These annealing conditions are comparable to those in Fig. 2: (A) $T_a = 115$°C; (B) 120°C; (C) 123°C; (D) 126°C.

causes large differences in the series of the DSC melting curve shapes, especially at the middle T_a range, compared to those for the shorter t_as. For 30-min annealing at $T_a =$ 120–122°C, the low-temperature peak becomes predominant, in contrast to the largest area of the high-temperature peak for the shorter annealing.

3.3. Morphological changes induced by annealing

Annealing also changes the lamellar morphologies, depending on the temperature and the time. Figs. 3–5 exhibit the series of TEM images of an initial unannealed mat and the sample annealed at different T_as for 1, 5 and 30 min, respectively. The gradual changes in the lamellar arrangement are visible, especially at the higher T_a. The initial unannealed structure shows the regular stacking of the single crystalline lamellae which are alternatively sandwiched between the dark layers indicating an amorphous region. These lamellae have a ~12.0-nm thickness. Such a lamellar structure laterally expanded through several-μm length, which was found from low-magnification images (not shown here).

At the lower $T_a = 115$°C, the regular stacking of the initial lamellar morphology is maintained even after 30-min annealing, as shown in Fig. 5. However, the thickness of each the lamella gradually increases from 12.3 nm for 1 min to 14.4 nm for 30-min annealing with increasing t_a. Increasing T_a up to 120°C causes coexistence of a small amount of the other type of rapidly rearranged lamellae, which has approximately a double thickness of around 20.0 nm. The characteristics of these "doubled" lamellae lie in their lateral dimension. Both the initial unannealed and the low $T_a = 115$°C annealed morphologies have a large size (several μm) in the lateral direction of the single-crystalline lamellae. However, at $T_a = 120$°C, the lateral dimension of the rearranged lamellae having a double thickness is restricted within 130-nm width. This phenomenon is especially obvious for $t_a = 30$ min (see Fig. 5).

The middle T_a range of 123°C produces a larger amount of the doubled lamellae, compared to that at $T_a = 120$°C, for any t_a. This type of doubly rearranged lamellar morphology exhibits the alternative stacking of the thickened lamellae. It should be noted that the thickness of the gradually rearranged lamellae increases with the elongation of t_a from 16.4 nm for $t_a = 1$ min to 17.8 nm for 30 min; however, it never exceeds that of the doubly rearranged ones of around 19.6–21.6 nm, depending on t_a.

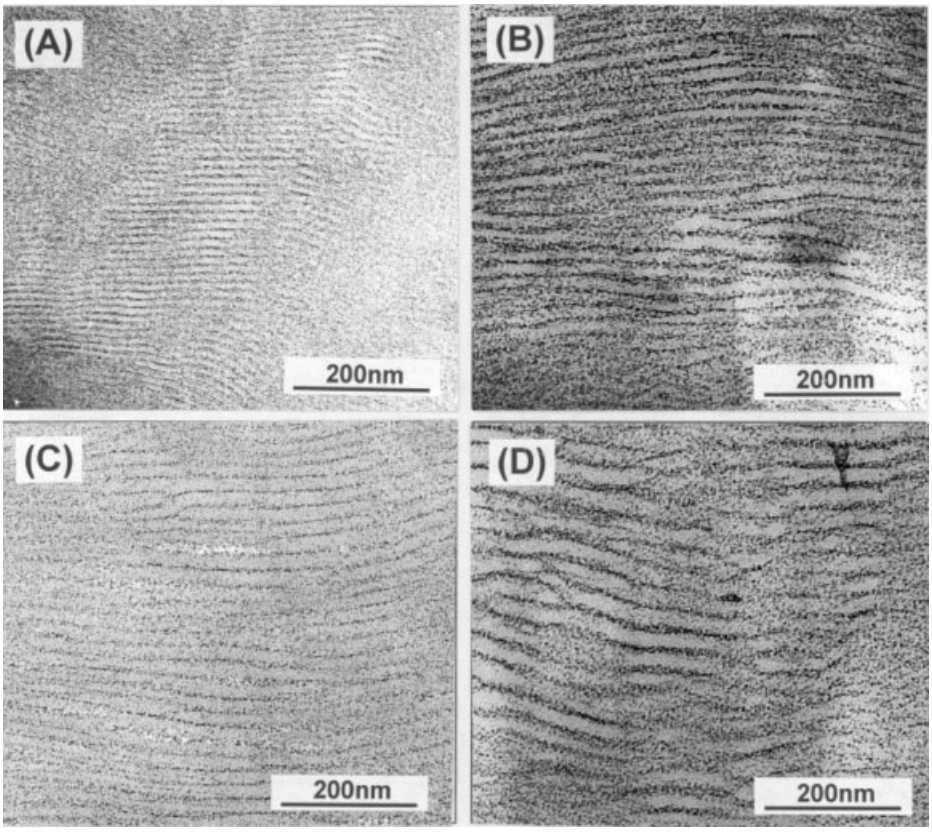

Fig. 5. TEM images of the sample annealed at different T_as for 30 min. These annealing conditions are comparable to those in Fig. 2: (A) $T_a = 115$°C; (B) 120°C; (C) 123°C; (D) 126°C.

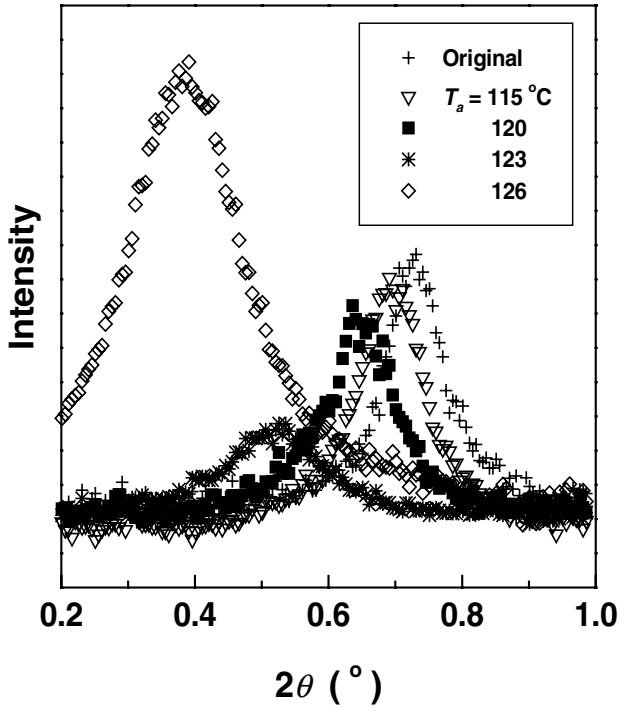

Fig. 6. SAXS intensity profiles for a series of unannealed and annealed samples. The background was subtracted from the original data plots. All these SAXS measurements were made at RT after the desired annealing for 5 min.

Further increase in T_a to 126°C causes the majority of the lamellae to be doubly rearranged at any t_a. Their lamellar thickness gradually increases with the increasing t_a from 23.3 nm for 1 min to 28.0 nm for 30 min. The limitation of the lateral dimension of such doubled lamellae also appears released with increasing t_a at this T_a range, that is their lateral continuity is gradually recovered from ~400 to ~620 nm wide at $T_a = 126$°C. Details of such a relationship between these morphologies reveled by the TEM observations and the DSC melting behavior are discussed later with the next results of the SAXS analysis.

3.4. X-ray scattering analysis

The periodicity change from the initial stacked lamellar morphology by annealing the samples was also confirmed by the SAXS measurements. Fig. 6 shows the SAXS profiles for the series of initial unannealed mat and samples annealed at 115–126°C for 5 min. These data were reduced from the imaging plate pattern having two scattering arcs along the equator perpendicular to the film surface. The line profiles on the equator are plotted in Fig. 6. The background of the incident beam was subtracted from the observed profiles. The profile of the initial unannealed single crystalline mat has a sharp peak located around $2\theta = 0.73°$

corresponding to its long period of ~12.0 nm, which shows a good agreement with the results obtained by the direct TEM observations (see previous section); crystalline and amorphous layers are alternative stacked with a regular periodicity. The sample annealed at a lower T_a of 115°C still shows a sharp long period peak, but the position slightly shifts to a lower 2θ angle around ~0.70°. (~12.7-nm long period). The rearrangement at this T_a region was limited to the gradual thickening of lamellae without any rapid lamellar doubling, as shown by TEM observation in Figs. 3–5. Thus, the periodicity of lamellar stacking is still retained at this T_a, which causes the sharp peak in Fig. 6. At T_a of 120°C, the SAXS long period peak further shifts to the lower 2θ side up to $2\theta = 0.65°$ (~13.6-nm long period); however, its intensity decreases. Here, it should be noted that the periodicity of the lamellae determines the SAXS intensity. The introduction of the small amount of the doubled lamellae causes a lack of periodicity of the lamellar stacking, which causes a reduction of the scattering peak intensity.

Suddenly at $T_a = 123$°C, only a broad scattering peak was detectable around $2\theta = 0.52°$. The direct TEM results in Figs. 3–5 have already clarified that this middle T_a range overlaps a two different types of lamellar rearrangement: a gradual lamellar thickening and a rapid lamellar doubling phenomena. Such resultant non-alternative stacking within the whole lamellae produces a broad profile for the sample annealed at this T_a range.

However, a further increase in T_a causes the recovery of the peak intensity. At T_a of 126°C, where the lamellar doubling was dominant as found from the TEM results, the SAXS long period peak around $2\theta = 0.38°$ has the highest intensity and a long period value of ~23.0 nm. A single type of lamellar reorganization causes the higher periodicity of the lamellar arrangement, leading to a re-growth of the SAXS peak intensity at $T_a = 126$°C in Fig. 6. This long period value is "doubled", compared to that of the unannealed original lamellae (~12 nm), which is also coincident with the TEM observation results shown in Fig. 3 for $t_a =$ 5 min.

Combination with the results obtained by the TEM observations can provide the above reasonable explanation for the SAXS change with the overlapping of different lamellar rearrangement mechanisms.

4. Discussion

4.1. Different rearrangement mechanisms

From the direct TEM observation results, it was found that the unannealed sample contains only the regular stacking of lamellae of ~12.0-nm thickness. However, there are two possible types of the lamellar rearrangements within the annealed materials: the *gradually* thickened lamellae holding their initial regular stacking and the *rapidly* doubled lamellae with their alternative stacking. Fig. 7 schematically represents the balance of these two rearrangement systems. At the lower T_a of 115°C, only the former type of rearranged lamellae was recognizable. Within the middle range of T_a from 120 to 123°C, both types of lamellae coexisted, which means that these two different rearrangement mechanisms overlapped. The intensity reduction of the SAXS long-period peak at this middle T_a range was caused by a lack of periodicity of the lamellar stacking, due to the combination of different lamellar arrangements within the sample. At the higher T_a of 126°C, the latter rearrangement became predominant in contrast to the negligible contribution of the former.

4.2. Assignment of three melting endotherms

The balance of these two rearrangement mechanisms seems to be controlled by annealing conditions (see Fig. 7). It could be quantified from the comparison of the DSC melting curves for the series of annealed samples. For evaluation of the relative amount of each type of the lamellar rearrangement, the endotherms should be assigned to the

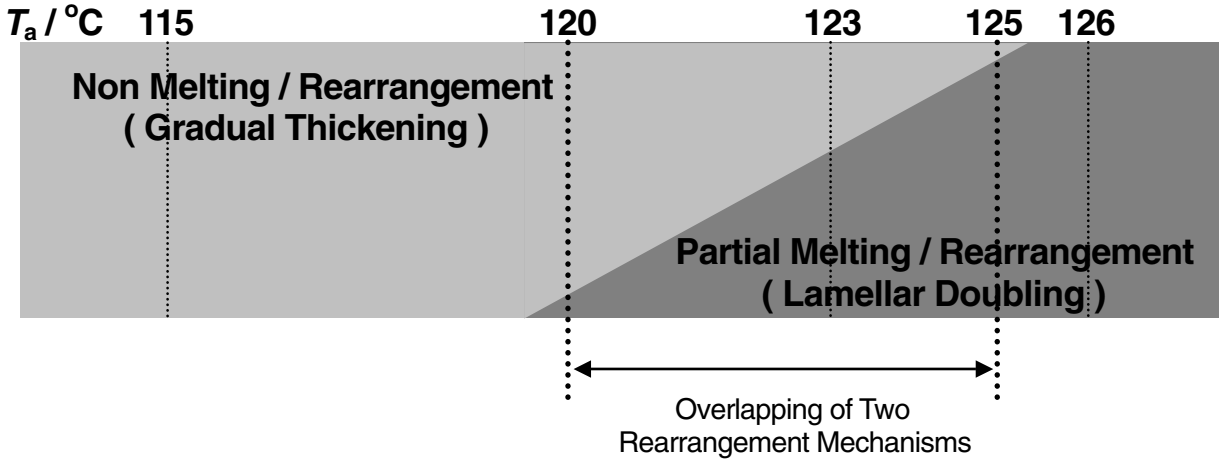

Fig. 7. Balance map of two rearrangement systems as a function of T_a.

melting of the lamellae rearranged through the corresponding mechanisms.

There were three possible categories of the melting peaks in this work: low-, middle- and high-temperature ones. The unannealed sample or that annealed at lowest T_a of 115°C has only two peaks, i.e., the low- and high-temperature peaks. The position of the low-temperature peak shifts due to annealing, but the high-temperature one retained its position. Here, the TEM results showed that there is only one type of lamellae which retains the initial regular stacking with a gradual increase in their thickness. Also, the T_a of 115°C is lower than the start of the melting endotherm even for the unannealed sample. Thus, the low-temperature peak can be assigned to the melting of the lamellae gradually thickened at T_a without any partial melting on annealing.

The middle-temperature peak appeared over $T_a = 120$°C, which exceeds the foot of the low-temperature endotherm of the unannealed sample. This indicates a slight but certain occurrence of partial melting during annealing at this T_a range. Correspondingly, the doubled lamellae having the alternative stacking were observed on the TEM images. Thus, the middle-temperature peak can be attributed to the melting of these lamellae reorganized through doubling which is accelerated by the partial melting of thinner lamellae.

On the other hand, the high-temperature peak is ascribed to the melting of the lamellae reorganized during the DSC heating scan because its position is not affected by whether annealing was applied or not. Finally, the high-temperature peak disappeared beyond a critical T_a around 123°C, which is coincident with the top of the low-temperature peak for the unannealed sample. This indicates that the lamellae are rearranged sufficiently through the gradual thickening or rapid doubling so as not to be more reorganizable during the DSC heating scans. In addition, the position of the middle-temperature peak at the higher $T_a = 126$°C approaches that of the high-temperature peak for the unannealed sample. This means that the lamellae whose melting corresponds to this high-temperature peak has been suddenly doubled during the non-isothermal annealing (continuous heating) process when the DSC scanning passes a critical T_a around 123°C, where the partial melting is dominant.

Such clear peak separations of the DSC profiles is impossible for a normal high density PE with a broad MW distribution, which shows a single but broad melting endotherm containing all of these three peaks.

4.3. Double melting peaks for the unannealed sample

These obtained results also provide an answer to the long-standing question concerning the HR dependence of the double endotherms. As shown in Fig. 1, even the initial unannealed sample exhibits an insignificant HR dependence of the positions of and balance between the low- and high-temperature peaks. These characteristics are coincident with the results obtained by Manley and coworkers [21]. However, if the low-temperature peak corresponds to the melting of the original lamellae, the higher intensity should be obtainable at the higher HR, which is not true in our case. The point lies in the relative progress between the lamellar rearrangement and the measured HR. That is, the lamellar doubling occurs quite rapidly, the speed of which exceeds the measured HR even if the highest HR of 80°C/min is used. With reaching the low-temperature peak during the DSC heating, only the small amount of the partial melting immediately accelerates the lamellar doubling so that it is impossible to melt all the initial lamellae without the doubling rearrangement. This is the reason that the low-temperature peak did not grow even at the higher HR in Fig. 1.

Indeed, the lower T_a annealing at 115°C, which is much lower than the peak position (~123°C) of this low-temperature endotherm for the initial unannealed sample, was effective for the higher-temperature side shift of the low-temperature peak even at the shorter t_a, as shown in Fig. 2. Thus, strictly speaking, the low-temperature peak should be ascribed to the melting of the lamellae slightly thickened from the "initial" lamellae during the DSC heating scan, but not to that of non-thickened lamellae.

Similarly, the high-temperature peak for the unannealed sample does not represent only one type of the lamellae having the same thickness. Actually, 1-min annealing exhibits the rapid doubling rearrangement over 120°C; thus, middle-temperature peaks should also exist even for a DSC profile of the unannealed sample at HR = 5°C/min because it takes 1 min for DSC heating from 120 to 125°C. Therefore, this high-temperature melting peak is composed of the "multiple" endotherms corresponding to the melting of all the lamellae rapidly rearranged at various temperatures over 120°C during the DSC heating.

4.4. Characteristics of the lamellar doubling rearrangement

A lamellar doubling rearrangement was allowed at a pair of two adjacent lamellae along a limited lateral length. Thus, the doubled lamellar regions were randomly distributed within the annealed sample at the lower T_a. Their amount increased with increasing T_a, which causes the growth of the middle-temperature peak in the DSC profiles. This doubling rearrangement may occur only for the stacked lamellae morphologies, such as the aggregation of single crystalline lamellae by filtering into the solution-crystallized mat prepared in this work, but not for a single lamella alone [22,23].

Hindered molecular sliding within the doubled lamellae might not favor the further division of the lateral dimension of the lamellae. Thus, the tripling or quadrupling of the lamellae was restrained, which could be confirmed by intensity reduction of the high-temperature peak, corresponding to the melting of the lamellae reorganized upon the DSC heating.

4.5. Evaluation of the overlapping rearrangements

Detection of such an overlapping of two different rearrangement mechanisms (see Fig. 7) may be difficult for analyzing by the scattering techniques alone, because their relative degree of proceeding cannot be evaluated from the lamellar periodicity. This is also true for our SAXS results. Sadler [17] has divided the rearrangement of single crystals of PE into two sections below and above $T_a = 123°C$. However, based on neutron scattering results, one can find only which rearrangement mechanism is predominant at a given T_a without showing their balance. Thus, the misunderstanding that there are strict T_a boundaries for these two rearrangement categories, not considering the possibility of their overlapping, has often been proposed. Our interpretation of these two overlapping reorganization systems could be followed by the combination of the resolved DSC endotherms and the TEM morphologies, reflecting the narrow MW distribution of our PE sample.

5. Conclusions

Two reorganization mechanisms for the stacked morphology of PE single crystals on annealing was revealed by the DSC and the SAXS measurements and by the TEM observations for the solution-crystallized PE. Although the unannealed sample had a very narrow distribution of lamellar thickness, which could be directly evaluated from the TEM images, its DSC melting curve had two endotherms, corresponding to the melting of initial lamellae and that of the crystals reorganized during the DSC heating, respectively. No significant HR dependence of the melting curve shape showed that such a rearrangement occurred quite quickly during the DSC heating scan. The combination of the TEM and the DSC data enabled the following interpretation for the rearrangement mechanisms starting from the stacked lamellar morphology. With the low-temperature annealing, the gradual lamellar thickening with no melt was predominant. In contrast, the high-temperature annealing gave the rapid lamellar rearrangement induced by the accelerated molecular sliding within the lamellar crystals, due to the partial melting of the initial thin lamellae. However, these different systems were competitive at the middle T_a. Rearranged morphologies varied, depending on their balance at the given T_a. In the case of the former annealing process, the lamellae gradually thickened with increasing t_a. The latter rapidly develops the lamellar doubling. Coexistence of lamellae thickened through these different rearrangement mechanisms causes a significant reduction of the SAXS long period peak at the middle T_a of 123°C; however, the gradual domination of the latter reorganization system brings the re-growth of SAXS peak again at the higher T_a of 126°C. Here, the limitation of the lateral dimension is recognizable for the doubling behavior with the alternative stacking of thickened lamellae.

References

[1] Wunderlich B. Macromolecular physics. New York: Academic Press, 1976.
[2] Bassett DC. Principles of polymer morphology. London: Cambridge University Press, 1981.
[3] Uehara H, Yamanobe T, Komoto T. Macromolecules 2000;33: 4861.
[4] Rastogi S, Spoelstra AB, Goossens JGP, Lemstra PJ. Macromolecules 1997;30:7880.
[5] Sadler DM, Spells SJ. Macromolecules 1989;22:3941.
[6] Spells SJ, Sadler DM. Macromolecules 1989;22:3948.
[7] Spells SJ, Hill MJ. Polymer 1991;32:2716.
[8] Mandelkern L, Sharma RK, Jackson JF. Macromolecules 1969;2:644.
[9] Kawaguchi A, Ichida T, Murakami S, Katayama K. Colloid Polym Sci 1984;262:597.
[10] Grubb DT, Liu JJH, Caffrey M, Bilderback DH. J Polym Sci, Polym Phys Ed 1984;22:367.
[11] Ichida T, Tsuji M, Murakami S, Kawaguchi A, Katayama K. Colloid Polym Sci 1985;263:293.
[12] Schultz JM, Fischer EW, Schaumburg O, Zachmann HA. J Polym Sci, Polym Phys Ed 1980;18:239.
[13] Strobl GR, Schneider MJ, Voigt-Martin IG. J Polym Sci, Polym Phys Ed 1980;18:1361.
[14] Nakajima A, Hayashi S, Nishimura H. Kolloid Z Z Polym 1969;229:107.
[15] Blackadder DA, Lewell PA. Polymer 1970;11:659.
[16] Blackadder DA, Lewell PA. Polymer 1970;11:147.
[17] Sadler DM. Polym Commun 1985;26:204.
[18] Bai SJ, Huang YF, Wu CC, Young TF. J Phys Chem Solid 1999;60:1337.
[19] Synder RG, Scherer JR, Reneker DH, Colson PJ. Polymer 1982;23:1286.
[20] Alamo R, Madelkern L. J Polym Sci, Polym Phys Ed 1986;24:2087.
[21] Leung WM, Manley RStJ, Panaras AR. Macromolecules 1985;18:753.
[22] Nagai H, Kajikawa N. Polymer 1968;9:177.
[23] Roe RJ, Gieniewski C, Vadimsky RG. J Polym Sci, Polym Phys Ed 1973;11:1653.